



HAL
open science

Fermi Detection of a Luminous γ -ray Pulsar in Globular Cluster

C. C.P. Freire, A. A. Abdo, Marco Ajello, A. Allafort, Jean Ballet, Guido Barbiellini, D. Bastieri, K. Bechtol, R. Bellazzini, R. D. Blandford, et al.

► **To cite this version:**

C. C.P. Freire, A. A. Abdo, Marco Ajello, A. Allafort, Jean Ballet, et al.. Fermi Detection of a Luminous γ -ray Pulsar in Globular Cluster. *Science*, 2011, 334, pp.1107-1110. 10.1126/science.1207141 . in2p3-00656632

HAL Id: in2p3-00656632

<https://hal.in2p3.fr/in2p3-00656632>

Submitted on 1 Apr 2020

HAL is a multi-disciplinary open access archive for the deposit and dissemination of scientific research documents, whether they are published or not. The documents may come from teaching and research institutions in France or abroad, or from public or private research centers.

L'archive ouverte pluridisciplinaire **HAL**, est destinée au dépôt et à la diffusion de documents scientifiques de niveau recherche, publiés ou non, émanant des établissements d'enseignement et de recherche français ou étrangers, des laboratoires publics ou privés.

Fermi Detection of a Luminous γ -ray Pulsar in a Globular Cluster

The Fermi LAT Collaboration^{1,2}

¹ All authors with their affiliations appear at the end of this paper.

² Corresponding authors: P. C. C. Freire, pfreire@mpifr-bonn.mpg.de;
T. J. Johnson, tyrel.j.johnson@gmail.com; D. Parent, dmparent@gmail.com;
C. Venter, Christo.Venter@nwu.ac.za.

November 1, 2018

We report the Fermi Large Area Telescope detection of γ -ray (>100 megaelectronvolts) pulsations from pulsar J1823–3021A in the globular cluster NGC 6624 with high significance ($\sim 7\sigma$). Its γ -ray luminosity $L_\gamma = (8.4 \pm 1.6) \times 10^{34}$ ergs per second, is the highest observed for any millisecond pulsar (MSP) to date, and it accounts for most of the cluster emission. The non-detection of the cluster in the off-pulse phase implies that it contains < 32 γ -ray MSPs, not ~ 100 as previously estimated. The γ -ray luminosity indicates that the unusually large rate of change of its period is caused by its intrinsic spin-down. This implies that J1823–3021A has the largest magnetic field and is the youngest MSP ever detected, and that such anomalous objects might be forming at rates comparable to those of the more normal MSPs.

Since its launch in 2008, the Large Area Telescope (LAT) on board the Fermi Gamma-ray Space Telescope (*F*) has detected whole populations of objects previously unseen in the γ -ray band. These include globular clusters (GCs), which are ancient spherical groups of \sim

19 10^5 stars held together by their mutual gravity. As a class, their γ -ray spectra show evidence
20 for an exponential cut-off at high energies (2, 3), a characteristic signature of magnetospheric
21 pulsar emission. This is not surprising because radio surveys have shown that GCs contain
22 large numbers of pulsars (4), neutron stars that emit radio and in some cases X-ray and γ -ray
23 pulsations.

24 The first GC detected at γ -ray energies was 47 Tucanae (5), soon followed by Terzan 5 (6)
25 and nine others (2, 3). Even so, no individual pulsars in these clusters were firmly identified
26 in γ -rays (7). GCs are more distant than most γ -ray pulsars observed in the Galactic disk (8),
27 thus most pulsars in them should be too faint to be detected individually. The Fermi LAT lacks
28 the spatial resolution required to resolve the pulsars in GCs, which tend to congregate within
29 the inner arcminute of the cluster. Hence, γ -ray photons emitted by all pulsars in a given GC
30 increase the photon background in the folded γ -ray profiles of each individual pulsar in that
31 cluster.

32 One of the GCs detected at γ -ray energies is NGC 6624 (3), located at a distance $d =$
33 8.4 ± 0.6 kpc from Earth (9). With a radio flux density at 400 MHz of $S_{400} = 16$ mJy (10),
34 J1823–3021A is the brightest of the six pulsars known in the cluster. It has been regularly
35 timed with the Jodrell Bank and Parkes radio telescopes since discovery, and with the Nançay
36 radio telescope since the launch of the Fermi satellite. The resulting radio ephemeris (Table
37 S1) describes the measured pulse times of arrival very well for the whole length of the Fermi
38 mission, the root mean square of the timing residuals being 0.1% of the pulsar rotational period.

39 Thus we can confidently use it to assign a pulsar spin phase ϕ to every γ -ray (>0.1 GeV)
40 photon arriving at the Fermi-LAT from the direction (within 0.8°) of the pulsar. We selected
41 photons that occurred between 4 August 2008 and 4 October 2010 that pass the “Pass 6 diffuse”
42 γ -ray selection cuts (1). The resulting pulsed γ -ray signal (above 0.1 GeV, Fig. 1) is very robust,
43 with an H-test value of 64 (11) corresponding to 6.8σ significance. The data are well modeled

44 by a power law with spectral index 1.4 ± 0.3 and an exponential cutoff at an energy of $1.3 \pm$
 45 0.6 GeV, typical of the values found for other γ -ray pulsars [see supporting online material
 46 (SOM)]. The two peaks are aligned, within uncertainties, with the two main radio components
 47 at spin phases $\phi_1 = 0.01 \pm 0.01$ and $\phi_2 = 0.64 \pm 0.01$ (Fig. 1).

48 The pulsed flux above 0.1 GeV, averaged over time, is $F_\gamma = (1.1 \pm 0.1 \pm 0.2) \times 10^{-11}$ erg cm $^{-2}$ s $^{-1}$,
 49 where the first errors are statistical and the second are systematic (SOM). The large distance
 50 of NGC 6624 implies that J1823–3021A is one of the most distant γ -ray pulsars detected
 51 (8). This makes it the most luminous γ -ray MSP to date (12): Its total emitted power is
 52 $L_\gamma = 4\pi d^2 f_\Omega F_\gamma = (8.4 \pm 1.6 \pm 1.5) \times 10^{34} (f_\Omega/0.9)$ erg s $^{-1}$. We obtained the statistical un-
 53 certainty by adding the uncertainties of d and F_γ in quadrature. The term f_Ω is the power per
 54 unit surface across the whole sky divided by power per unit surface received at Earth’s location;
 55 detailed modeling of the γ and radio light curves provides a best fit centered at 0.9, but with a
 56 possible range from 0.3 to 1.8 (SOM).

57 The LAT image of the region around NGC 6624 during the on-pulse interval ($0.60 < \phi <$
 58 0.67 and $0.90 < \phi < 1.07$) shows a bright and isolated γ -ray source that is consistent with the
 59 location of J1823–3021A (Fig. 2); in the off-pulse region ($0.07 < \phi < 0.60$ and $0.67 < \phi <$
 60 0.90) no point sources in the energy band 0.1 - 100 GeV are detectable. Assuming a typical
 61 pulsar spectrum with a spectral index of 1.5 and a cut-off energy of 3 GeV, we derived, after
 62 scaling to the full pulse phase, a 95% confidence level upper limit on the point source energy
 63 flux of 5.5×10^{-12} erg cm $^{-2}$ s $^{-1}$. Thus, J1823–3021A dominates the total γ -ray emission of
 64 the cluster. The combined emission of all other MSPs in the cluster plus any off-pulse emission
 65 from J1823–3021A is not detectable with present sensitivity. No other pulsars are detected in
 66 a pulsation search either.

67 Under the assumption that the γ -ray emission originates from NGC 6624, (3) estimated the
 68 total number of MSPs to be $N_{\text{MSP}} = 103_{-46}^{+104}$. Assuming an average γ -ray luminosity for each

69 MSP (5, 2), similar to the approximation made by (3), our off-pulse flux upper limit implies that
70 $N_{\text{MSP}} < 32$. This is consistent with the estimate $N_{\text{MSP}} = 30 \pm 15$ derived from the correlation
71 between γ -ray luminosity and encounter rate (2). Clearly, the MSP number estimate of (3) is
72 skewed by the presence of a single bright pulsar contributing disproportionately to its emission
73 (13). The off-pulse emission limits can also be used to constrain alternative models for the γ -ray
74 emission from globular clusters, like those invoking inverse Compton (IC) radiation (14, 15).

75 The spin period of J1823–3021A, 5.44 ms, is typical of MSPs. However, its rate of change
76 $\dot{P}_{\text{obs}} = +3.38 \times 10^{-18} \text{ s s}^{-1}$ is one to two orders of magnitude larger than for other MSPs with
77 the exception of J1824–2452A, a pulsar in the GC M28 (16) that has a similarly large \dot{P}_{obs} (17).
78 A possible explanation is that \dot{P}_{obs} is due mostly to the changing Doppler shift caused by the
79 pulsar’s acceleration in the gravitational field of the cluster along the line of sight (a_l):

$$\left(\frac{\dot{P}_{\text{obs}}}{P}\right) = \left(\frac{\dot{P}}{P}\right) + \frac{a_l}{c}. \quad (1)$$

80 If the globular cluster has a reliable mass model, we could use it to estimate lower and upper
81 limits for a_l and estimate upper and lower limits for \dot{P} (18). For NGC 6624 the collapsed nature
82 of its core precludes the derivation of a reliable mass model. Furthermore, radio timing (Table
83 S1) shows that J1823–3021A is only $0'.4 \pm 0'.1$ (a projected distance of 0.018 ± 0.004 pc)
84 from the center of the cluster (19), where the values of a_l can be largest. For this reason, it
85 has been suggested (10) that J1823–3021A is a “normal” MSP (i.e., with small \dot{P}); its large
86 \dot{P}_{obs} being due to its acceleration in the cluster. This conclusion was apparently strengthened
87 by the detection of a second derivative of the spin period $\ddot{P} = -1.7 \times 10^{-29} \text{ s}^{-1}$ (20). This
88 could originate in a time variation of a_l resulting from interaction with a nearby object (21). If
89 sustained it would reverse the sign of \dot{P}_{obs} in ~ 6000 years; suggesting again that the large \dot{P}_{obs}
90 is not only due to dynamical effects, but is possibly a transient feature.

91 However, the total observed γ -ray emission L_γ must represent a fraction $\eta < 1$ of the

92 available rotational energy loss, $\dot{E} = 4\pi^2 I \dot{P} / P^3$, where I is the pulsar's moment of inertia.
 93 Although I depends on the unknown mass of the pulsar and the unknown equation of state for
 94 dense matter, the standard assumption $I = 10^{45} \text{ g cm}^2$ is a reasonable value for a $1.4 M_\odot$ (mass
 95 of the Sun) neutron star. This implies $\dot{P} > 3.4 \times 10^{-19} (f_\Omega/0.9)(I/10^{45} \text{ g cm}^2)^{-1} \text{ s s}^{-1}$. Thus
 96 even an unrealistic γ -ray efficiency $\eta = 1$ would imply that \dot{P} is already $\sim 10\%$ of \dot{P}_{obs} . If we
 97 assume instead $\dot{P} \simeq \dot{P}_{\text{obs}}$, then $\dot{E} = 8.3 \times 10^{35} \text{ erg s}^{-1}$ and $\eta = 0.1 \times (f_\Omega/0.9)(I/10^{45} \text{ g cm}^2)^{-1}$.
 98 Comparison with the observed γ -ray efficiencies of other MSPs (12, 8) shows this to be a more
 99 reasonable range of values; $\eta \sim 0.1$ also represents the upper limit derived for the average effi-
 100 ciency of MSPs in 47 Tucanae (5). Therefore, our γ -ray detection of J1823–3021A indicates
 101 that it is unusually energetic and that most of \dot{P}_{obs} is due to its intrinsic spin-down. The pulsar
 102 has other features that suggest it is indeed unusually energetic: Its alignment of radio and γ -ray
 103 profiles has previously only been observed for the Crab pulsar (22) and three fast, energetic
 104 MSPs: J1939+2134 (the first MSP to be discovered), J1959+2048 (23) and J0034–0534 (24).
 105 Like some of these energetic pulsars and PSR J1824–2452A, J1823–3021A emits giant radio
 106 pulses (25) and has a high 400 MHz radio luminosity of $L_{400} \simeq 1.1 \text{ Jy kpc}^2$ (10), the third
 107 highest among known MSPs. However the correlation between \dot{E} and radio luminosity is far
 108 from perfect given the uncertainties in the distance estimates, moment of inertia, beaming ef-
 109 fects and possibly intrinsic variations of the emission efficiencies. Finally, J1939+2134 also has
 110 a large \ddot{P} (26), which is thought to be caused by timing noise (TN), which scales roughly with
 111 $P^{-1.1} \dot{P}$ (27). In the case of J1823–3021A, if $\dot{P} \simeq \dot{P}_{\text{obs}}$, then TN should be one order of mag-
 112 nitude larger than for J1939+2134; instead its \ddot{P} is $\sim 1.5 \times 10^2$ larger than that of J1939+2134.
 113 This is possible given the observed scatter around the TN scaling law. Thus TN might account
 114 for the \ddot{P} of J1823–3021A, but this is far more likely if $\dot{P} \simeq \dot{P}_{\text{obs}}$.

115 If $\dot{P} \simeq \dot{P}_{\text{obs}}$, we can estimate the strength of its surface dipole magnetic field: $B_0 = 3.2 \times$
 116 $10^{19} \text{ G} \sqrt{\dot{P} P (I/10^{45} \text{ g cm}^2) (R/10 \text{ km})^{-3}} \simeq 4.3 \times 10^9 \text{ G}$ (28) [where R is the neutron star (NS)

117 radius, generally assumed to be 10 km]. MSPs are thought to start as normal NSs with $B_0 \sim$
 118 10^{11-13} G which are then spun up by the accretion of matter and angular momentum from a
 119 companion star. This process is thought to decrease their magnetic field to $B_0 \sim 10^{7-9}$ G; but
 120 the exact mechanism responsible for this is currently not well understood. Our value of B_0
 121 shows that for J1823–3021A this decrease was not as pronounced as for other MSPs.

122 As accretion spins up the NS, it eventually reaches an equilibrium spin period (29) given
 123 by:

$$P_{\text{init}} = 2.4\text{ms} \left(\frac{B_0}{10^9\text{G}} \right)^{6/7} \left(\frac{M}{M_\odot} \right)^{-5/7} \left(\frac{R}{10^4\text{m}} \right)^{18/7} \left(\frac{\dot{M}}{\dot{M}_{\text{Edd}}} \right)^{-3/7}, \quad (2)$$

124 where M is the NS mass, \dot{M} is the accretion rate and \dot{M}_{Edd} is the maximum possible stable ac-
 125 cretion rate for a spherical configuration (known as the Eddington rate). Beyond this, the pres-
 126 sure of accretion-related radiation starts preventing further accretion. After accretion ceases,
 127 the newly formed radio MSP will have P_{init} as its initial spin period. Assuming $\dot{M} = \dot{M}_{\text{Edd}}$,
 128 $M = 1.4 M_\odot$ and $R = 10$ km (as in our estimates of B_0), we obtain $P_{\text{init}} = 1.9 \text{ ms}(B_0/10^9\text{G})^{6/7}$.
 129 For the value of B_0 calculated above, we get $P_{\text{init}} = 6.6$ ms; that is, even if accretion had
 130 proceeded at the Eddington rate, the pulsar would not have been spun up to its present spin
 131 frequency. This is also the case for the other such “anomalous” MSP, J1824–2452A (17); for
 132 all others we have $P > P_{\text{init}}$. A possible explanation is that for these two objects M and I
 133 do not correspond to the assumptions above. If, for example, $\eta = 0.15$, $M = 1.8 M_\odot$ and
 134 $I = 1.8 \times 10^{45} \text{ g cm}^2$ (30) we obtain $B_0 = 3.6 \times 10^9$ G and $P_{\text{init}} = 4.7$ ms. A second possibil-
 135 ity, suggested by eq. 2, is super-Eddington accretion (more precisely, $\dot{M} > 1.6 \dot{M}_{\text{Edd}}$); this can
 136 happen for non-spherical mass accretion. A third possibility is that the value of B_0 was smaller
 137 during accretion (resulting in a smaller P_{init}), and that B_0 has increased since then. This has
 138 been observed for some normal pulsars (31); however there is no evidence of such behavior for
 139 any other MSPs.

140 In any case, the conclusion that $\dot{P} \simeq \dot{P}_{\text{obs}}$ implies a characteristic age $\tau_c = P/(2\dot{P}) = 25$
141 million years. This is likely an over-estimate of the true age of the pulsar, particularly given
142 that P_{init} is likely to be similar to P . Thus J1823–3021A is likely to be the youngest MSP ever
143 detected; only J1824–2452A might have a comparable age. Because of their large \dot{P} s both
144 objects will be observable as MSPs for a time that is $\sim 10^2$ shorter than the ~ 100 “normal”
145 radio-bright MSPs known in GCs. Statistically, this suggests that, at least in GCs, anomalous
146 high B -field MSPs like J1823–3021A and J1824–2452A are forming at rates comparable to
147 those of the more “normal”, radio-bright MSPs.

148 **References and Notes**

- 149 1. W. B. Atwood *et al.*, *Astrophys. J.* **697**, 1071 (2009).
- 150 2. A. A. Abdo *et al.*, *Astron. & Astrophys.* **524**, A75 (2010).
- 151 3. P. H. T. Tam *et al.*, *Astrophys. J.* **729**, 90 (2011).
- 152 4. See updated list of pulsars in globular clusters and references in
153 <http://www.naic.edu/~pfreire/GCpsr.html>.
- 154 5. A. A. Abdo *et al.*, *Science* **325**, 845 (2009).
- 155 6. A. K. H. Kong *et al.* *Astrophys. J.* **712**, L36 (2010).
- 156 7. The AGILE collaboration reported a low-significance detection of the MSP J1824–2452A
157 in the globular cluster M28 that has not been confirmed (32).
- 158 8. A. A. Abdo *et al.*, *Astrophys. J. Supp.* **187**, 460 (2010).
- 159 9. E. Valenti, F. R. Ferraro, L. Origlia, *Astron. J.* **133**, 1287 (2007).

- 160 10. J. D. Biggs *et al.*, *Mon. Not. R. Astron. Soc.* **267**, 125 (1994).
- 161 11. O. C. de Jager, I. Büsching, *Astron. & Astrophys.* **517**, L9 (2010).
- 162 12. A. A. Abdo *et al.* (Fermi-LAT collaboration), *Science* **325**, 848 (2009).
- 163 13. A. S. Fruchter & W. M. Goss, *Astrophys. J.* **536**, 865 (2000).
- 164 14. W. Bednarek, J. Sitarek, *Mon. Not. R. Astron. Soc.* **377**, 920 (2007).
- 165 15. K. S. Cheng *et al.* *Astrophys. J.* **723**, 1219 (2010).
- 166 16. A. G. Lyne *et al.*, *Nature* **328**, 399 (1987).
- 167 17. R. S. Foster *et al.* *Astrophys. J.* **326**, L13 (1988).
- 168 18. P. C. Freire, *et al.*, *Mon. Not. R. Astron. Soc.* **340**, 1359 (2003).
- 169 19. R. Goldsbury, *et al.*, *Astron. J.* **140**, 1830 (2010).
- 170 20. G. Hobbs *et al.* *Mon. Not. R. Astron. Soc.* **353**, 1311 (2004).
- 171 21. E. S. Phinney, *Royal Society of London Philosophical Transactions Series A* **341**, 39 (1992).
- 172 22. A. A. Abdo, *et al.*, *Astrophys. J.* **708**, 1254 (2010).
- 173 23. L. Guillemot, *et al.*, arXiv:1101.0669 (2011).
- 174 24. A. A. Abdo, *et al.*, *Astrophys. J.* **712**, 957 (2010).
- 175 25. H. S. Knight, *Mon. Not. R. Astron. Soc.* **378**, 723 (2007).
- 176 26. Cognard, I., Bourgois, G., Lestrade, J.-F., et al. 1995, *Astron. & Astrophys.* **296**, 169 (1995)
- 177 27. Shannon, R. M., & Cordes, J. M., *Astrophys. J.* **725**, 1607 (2010).

- 178 28. Lorimer, D. R., & Kramer, M. Handbook of pulsar astronomy, by D. R. Lorimer and
179 M. Kramer. Cambridge observing handbooks for research astronomers, Vol. 4. Cambridge,
180 UK: Cambridge University Press (2004).
- 181 29. M. A. Alpar, A. F. Cheng, M. A. Ruderman, & J. Shaham, *Nature* **300**, 728 (1982).
- 182 30. Worley, A., Krastev, P. G., & Li, B.-A., *Astrophys. J.* **685**, 390 (2008)
- 183 31. C. Espinoza *et al.* arXiv:1109.2740 (2011).
- 184 32. A. Pellizzoni *et al.*, *Astrophys. J.* **695**, L115 (2009)
- 185 33. D. A. Smith, *et al.*, *Astron. & Astrophys.* **492**, 923 (2008).
- 186 34. G. Hobbs *et al.* *Mon. Not. R. Astron. Soc.* **353**, 1311 (2004).
- 187 35. I. Cognard, G. Theureau, G. Desvignes, R. Ferdman, arXiv:0911.1612 (2009).
- 188 36. G. B. Hobbs, *et al.*, *Mon. Not. R. Astron. Soc.* **369**, 655 (2006).
- 189 37. W. B. Atwood, *et al.* (Fermi-LAT collaboration), *Astrophys. J.* **697**, 1071 (2009).
- 190 38. P. S. Ray, M. Kerr, D. Parent *et al.*, *Astrophys. J. Supp.* **194**, 17 (2011).
- 191 39. A. A. Abdo, *et al.* (Fermi-LAT collaboration), *Astrophys. J. Supp.* **188**, 405 (2010).
- 192 40. A. A. Abdo, *et al.* (Fermi-LAT collaboration), *Astrophys. J. Supp.* **187**, 460 (2010).
- 193 41. A. A. Abdo, *et al.* (Fermi-LAT collaboration), *Astron. & Astrophys.* **524**, A75 (2010).
- 194 42. P. H. T. Tam *et al.*, *Astrophys. J.* **729**, 90 (2011).
- 195 43. J. K. Daugherty, A. K. Harding, *Astrophys. J.* **252**, 337 (1982).
- 196 44. J. K. Daugherty, A. K. Harding, *Astrophys. J.* **458**, 278 (1996).

- 197 45. K. S. Cheng, C. Ho, M. Ruderman, *Astrophys. J.* **300**, 500 (1986a).
- 198 46. K. S. Cheng, C. Ho, M. Ruderman, *Astrophys. J.* **300**, 522 (1986b).
- 199 47. R. W. Romani, *Astrophys. J.* **470**, 469 (1996).
- 200 48. J. Arons, *Astrophys. J.* **266**, 215 (1983).
- 201 49. J. Dyks, B. Rudak, *Astrophys. J.* **598**, 1201 (2003).
- 202 50. M. Morini, *Mon. Not. R. Astron. Soc.* **202**, 495 (1983).
- 203 51. K. P. Watters, R. W. Romani, *et al.* *Astrophys. J.* **695**, 1289 (2009).
- 204 52. C. Venter, A. K. Harding, & L. Guillemot, *Astrophys. J.* **707**, 800 (2009).
- 205 53. A. A. Abdo *et al.* (Fermi-LAT collaboration), *Astrophys. J.* **712**, 957 (2010).
- 206 54. I. H. Stairs, S. E. Thorsett, & F. Camilo, *Astrophys. J. Supp.* **123**, 627 (1999).
- 207 55. T. J. Johnson, Ph. D. Thesis, University of Maryland, College Park, U.S.A. (2011).

208 The Fermi-LAT Collaboration acknowledges support from a number of agencies and in-
209 stitutes for both development and the operation of the LAT as well as scientific data analy-
210 sis. These include NASA and the Department of Energy in the United States; Commissariat
211 à l’Energie Atomique et aux Énergies Alternatives / Institut de Recherche sur les Lois Funda-
212 mentales de l’Univers (CEA/IRFU) and Institut National de Physique Nucléaire et de Physique
213 des Particules, Centre National de la Recherche Scientifique (IN2P3/CNRS) in France; Agen-
214 zia Spaziale Italiana (ASI) and Istituto Nazionale di Fisica Nucleare (INFN) in Italy; Min-
215 istry of Education, Culture, Sports, Science and Technology (MEXT), Energy Accelerator Re-
216 search Organization (KEK), and Japan Aerospace Exploration Agency (JAXA) in Japan; and
217 the K. A. Wallenberg Foundation, Swedish Research Council and the National Space Board in

218 Sweden. Additional support from Istituto Nazionale di Astrofisica (INAF) in Italy and Cen-
219 tre National d’Etudes Spaciales (CNES) in France for science analysis during the operations
220 phase is also gratefully acknowledged. The Nançay Radio Observatory is operated by the Paris
221 Observatory, associated with the CNRS. The Lovell Telescope is owned and operated by the
222 University of Manchester as part of the Jodrell Bank Centre for Astrophysics with support from
223 the Science and Technology Facilities Council of the United Kingdom. Fermi LAT data, γ -ray
224 diffuse models, and radio pulsar ephemeris are available from the Fermi Science Support Cen-
225 ter (<http://fermi.gsfc.nasa.gov/ssc/data/access>). We also thank the anonymous referees and the
226 Science editors for the very constructive suggestions.

227 **The Fermi LAT Collaboration:** P. C. C. Freire¹, A. A. Abdo², M. Ajello³, A. Allafort³,
228 J. Ballet⁴, G. Barbiellini^{5,6}, D. Bastieri^{7,8}, K. Bechtol³, R. Bellazzini⁹, R. D. Blandford³, E. D. Bloom³,
229 E. Bonamente^{10,11}, A. W. Borgland³, M. Brigida^{12,13}, P. Bruel¹⁴, R. Buehler³, S. Buson^{7,8},
230 G. A. Caliandro¹⁵, R. A. Cameron³, F. Camilo¹⁶, P. A. Caraveo¹⁷, C. Cecchi^{10,11}, Ö. Çelik^{18,19,20},
231 E. Charles³, A. Chekhtman²¹, C. C. Cheung²², J. Chiang³, S. Ciprini^{23,11}, R. Claus³, I. Cognard²⁴,
232 J. Cohen-Tanugi²⁵, L. R. Cominsky²⁶, F. de Palma^{12,13}, C. D. Dermer²⁷, E. do Couto e Silva³,
233 M. Dormody²⁸, P. S. Drell³, R. Dubois³, D. Dumora²⁹, C. M. Espinoza³⁰, C. Favuzzi^{12,13},
234 S. J. Fegan¹⁴, E. C. Ferrara¹⁸, W. B. Focke³, P. Fortin¹⁴, Y. Fukazawa³¹, P. Fusco^{12,13}, F. Gargano¹³,
235 D. Gasparri³², N. Gehrels¹⁸, S. Germani^{10,11}, N. Giglietto^{12,13}, F. Giordano^{12,13}, M. Giroletti³³,
236 T. Glanzman³, G. Godfrey³, I. A. Grenier⁴, M.-H. Grondin^{34,35}, J. E. Grove²⁷, L. Guillemot¹,
237 S. Guiriec³⁶, D. Hadasch¹⁵, A. K. Harding¹⁸, G. Jóhannesson³⁷, A. S. Johnson³, T. J. Johnson^{18,22,46,2},
238 S. Johnston³⁸, H. Katagiri³⁹, J. Kataoka⁴⁰, M. Keith³⁸, M. Kerr³, J. Knödseder^{41,3}, M. Kramer^{30,1},
239 M. Kuss⁹, J. Lande³, L. Latronico⁴³, S.-H. Lee⁴⁴, M. Lemoine-Goumard^{29,45}, F. Longo^{5,6},
240 F. Loparco^{12,13}, M. N. Lovellette²⁷, P. Lubrano^{10,11}, A. G. Lyne³⁰, R. N. Manchester³⁸, M. Marelli¹⁷,
241 M. N. Mazziotta¹³, J. E. McEnery^{18,46}, P. F. Michelson³, T. Mizuno³¹, A. A. Moiseev^{19,46},
242 C. Monte^{12,13}, M. E. Monzani³, A. Morselli⁴⁷, I. V. Moskalenko³, S. Murgia³, T. Nakamori⁴⁰,

243 P. L. Nolan³, J. P. Norris⁴⁸, E. Nuss²⁵, T. Ohsugi⁴⁹, A. Okumura^{3,50}, N. Omodei³, E. Orlando^{3,51},
244 M. Ozaki⁵⁰, D. Paneque^{52,3}, D. Parent², M. Pesce-Rollins⁹, M. Pierbattista⁴, F. Piron²⁵, T. A. Porter³,
245 S. Rainò^{12,13}, S. M. Ransom⁵³, P. S. Ray²⁷, A. Reimer^{54,3}, O. Reimer^{54,3}, T. Reposeur²⁹, S. Ritz²⁸,
246 R. W. Romani³, M. Roth⁵⁵, H. F.-W. Sadrozinski²⁸, P. M. Saz Parkinson²⁸, C. Sgrò⁹, R. Shannon³⁸,
247 E. J. Siskind⁵⁶, D. A. Smith²⁹, P. D. Smith⁵⁷, P. Spinelli^{12,13}, B. W. Stappers³⁰, D. J. Suson⁵⁸,
248 H. Takahashi⁴⁹, T. Tanaka³, T. M. Tauris^{59,1}, J. B. Thayer³, G. Theureau²⁴, D. J. Thompson¹⁸,
249 S. E. Thorsett⁶⁰, L. Tibaldo^{7,8}, D. F. Torres^{15,61}, G. Tosti^{10,11}, E. Troja^{18,62}, J. Vandenbroucke³,
250 A. Van Etten³, V. Vasileiou²⁵, C. Venter⁶³, G. Vianello^{3,64}, N. Vilchez^{41,42}, V. Vitale^{47,65}, A. P. Waite³,
251 P. Wang³, K. S. Wood²⁷, Z. Yang^{66,67}, M. Ziegler²⁸, S. Zimmer^{66,67}

252

253 ¹ Max-Planck-Institut für Radioastronomie, Auf dem Hügel 69, 53121 Bonn, Germany. ²
254 Center for Earth Observing and Space Research, College of Science, George Mason Univer-
255 sity, Fairfax, VA 22030, resident at Naval Research Laboratory, Washington, DC 20375, USA.
256 ³ W. W. Hansen Experimental Physics Laboratory, Kavli Institute for Particle Astrophysics
257 and Cosmology, Department of Physics and SLAC National Accelerator Laboratory, Stan-
258 ford University, Stanford, CA 94305, USA. ⁴ Laboratoire AIM, CEA-IRFU/CNRS/Université
259 Paris Diderot, Service d’Astrophysique, CEA Saclay, 91191 Gif sur Yvette, France. ⁵ Isti-
260 tuto Nazionale di Fisica Nucleare, Sezione di Trieste, I-34127 Trieste, Italy. ⁶ Dipartimento
261 di Fisica, Università di Trieste, I-34127 Trieste, Italy. ⁷ Istituto Nazionale di Fisica Nucleare,
262 Sezione di Padova, I-35131 Padova, Italy. ⁸ Dipartimento di Fisica “G. Galilei”, Università
263 di Padova, I-35131 Padova, Italy. ⁹ Istituto Nazionale di Fisica Nucleare, Sezione di Pisa, I-
264 56127 Pisa, Italy. ¹⁰ Istituto Nazionale di Fisica Nucleare, Sezione di Perugia, I-06123 Perugia,
265 Italy. ¹¹ Dipartimento di Fisica, Università degli Studi di Perugia, I-06123 Perugia, Italy. ¹²
266 Dipartimento di Fisica “M. Merlin” dell’Università e del Politecnico di Bari, I-70126 Bari,
267 Italy. ¹³ Istituto Nazionale di Fisica Nucleare, Sezione di Bari, 70126 Bari, Italy. ¹⁴ Labora-

268 toire Leprince-Ringuet, École polytechnique, CNRS/IN2P3, Palaiseau, France. ¹⁵ Institut de
269 Ciències de l'Espai (IEEE-CSIC), Campus UAB, 08193 Barcelona, Spain. ¹⁶ Columbia As-
270 trophysics Laboratory, Columbia University, New York, NY 10027, USA. ¹⁷ INAF-Istituto di
271 Astrofisica Spaziale e Fisica Cosmica, I-20133 Milano, Italy. ¹⁸ NASA Goddard Space Flight
272 Center, Greenbelt, MD 20771, USA. ¹⁹ Center for Research and Exploration in Space Science
273 and Technology (CRESST) and NASA Goddard Space Flight Center, Greenbelt, MD 20771,
274 USA. ²⁰ Department of Physics and Center for Space Sciences and Technology, University
275 of Maryland Baltimore County, Baltimore, MD 21250, USA. ²¹ Artep Inc., 2922 Excelsior
276 Springs Court, Ellicott City, MD 21042, resident at Naval Research Laboratory, Washing-
277 ton, DC 20375, USA. ²² National Research Council Research Associate, National Academy
278 of Sciences, Washington, DC 20001, resident at Naval Research Laboratory, Washington, DC
279 20375, USA. ²³ ASI Science Data Center, I-00044 Frascati (Roma), Italy. ²⁴ Laboratoire de
280 Physique et Chimie de l'Environnement, LPCE UMR 6115 CNRS, F-45071 Orléans Cedex
281 02, and Station de radioastronomie de Nançay, Observatoire de Paris, CNRS/INSU, F-18330
282 Nançay, France. ²⁵ Laboratoire Univers et Particules de Montpellier, Université Montpellier 2,
283 CNRS/IN2P3, Montpellier, France. ²⁶ Department of Physics and Astronomy, Sonoma State
284 University, Rohnert Park, CA 94928-3609, USA. ²⁷ Space Science Division, Naval Research
285 Laboratory, Washington, DC 20375-5352, USA. ²⁸ Santa Cruz Institute for Particle Physics,
286 Department of Physics and Department of Astronomy and Astrophysics, University of Cali-
287 fornia at Santa Cruz, Santa Cruz, CA 95064, USA. ²⁹ Université Bordeaux 1, CNRS/IN2p3,
288 Centre d'Études Nucléaires de Bordeaux Gradignan, 33175 Gradignan, France. ³⁰ Jodrell Bank
289 Centre for Astrophysics, School of Physics and Astronomy, The University of Manchester, M13
290 9PL, UK. ³¹ Department of Physical Sciences, Hiroshima University, Higashi-Hiroshima, Hi-
291 roshima 739-8526, Japan. ³² Agenzia Spaziale Italiana (ASI) Science Data Center, I-00044
292 Frascati (Roma), Italy. ³³ INAF Istituto di Radioastronomia, 40129 Bologna, Italy. ³⁴ Max-

293 Planck-Institut für Kernphysik, D-69029 Heidelberg, Germany. ³⁵ Landessternwarte, Univer-
294 sität Heidelberg, Königstuhl, D 69117 Heidelberg, Germany. ³⁶ Center for Space Plasma and
295 Aeronomic Research (CSPAR), University of Alabama in Huntsville, Huntsville, AL 35899,
296 USA. ³⁷ Science Institute, University of Iceland, IS-107 Reykjavik, Iceland. ³⁸ CSIRO As-
297 tronomy and Space Science, Australia Telescope National Facility, Epping NSW 1710, Aus-
298 tralia. ³⁹ College of Science, Ibaraki University, 2-1-1, Bunkyo, Mito 310-8512, Japan. ⁴⁰
299 Research Institute for Science and Engineering, Waseda University, 3-4-1, Okubo, Shinjuku,
300 Tokyo 169-8555, Japan. ⁴¹ CNRS, IRAP, F-31028 Toulouse cedex 4, France. ⁴² GAHEC,
301 Université de Toulouse, UPS-OMP, IRAP, Toulouse, France. ⁴³ Istituto Nazionale di Fisica Nu-
302 cleare, Sezioine di Torino, I-10125 Torino, Italy. ⁴⁴ Yukawa Institute for Theoretical Physics,
303 Kyoto University, Kitashirakawa Oiwake-cho, Sakyo-ku, Kyoto 606-8502, Japan. ⁴⁵ Funded
304 by contract ERC-StG-259391 from the European Community. ⁴⁶ Department of Physics and
305 Department of Astronomy, University of Maryland, College Park, MD 20742, USA. ⁴⁷ Istituto
306 Nazionale di Fisica Nucleare, Sezione di Roma “Tor Vergata”, I-00133 Roma, Italy. ⁴⁸ De-
307 partment of Physics, Boise State University, Boise, ID 83725, USA. ⁴⁹ Hiroshima Astrophys-
308 ical Science Center, Hiroshima University, Higashi-Hiroshima, Hiroshima 739-8526, Japan.
309 ⁵⁰ Institute of Space and Astronautical Science, JAXA, 3-1-1 Yoshinodai, Chuo-ku, Sagami-
310 hara, Kanagawa 252-5210, Japan. ⁵¹ Max-Planck Institut für extraterrestrische Physik, 85748
311 Garching, Germany. ⁵² Max-Planck-Institut für Physik, D-80805 München, Germany. ⁵³ Na-
312 tional Radio Astronomy Observatory (NRAO), Charlottesville, VA 22903, USA. ⁵⁴ Institut für
313 Astro- und Teilchenphysik and Institut für Theoretische Physik, Leopold-Franzens-Universität
314 Innsbruck, A-6020 Innsbruck, Austria. ⁵⁵ Department of Physics, University of Washington,
315 Seattle, WA 98195-1560, USA. ⁵⁶ NYCB Real-Time Computing Inc., Lattingtown, NY 11560-
316 1025, USA. ⁵⁷ Department of Physics, Center for Cosmology and Astro-Particle Physics, The
317 Ohio State University, Columbus, OH 43210, USA. ⁵⁹ Department of Chemistry and Physics,

318 Purdue University Calumet, Hammond, IN 46323-2094, USA. ⁵⁹ Argelander-Institut für As-
319 tronomie, Universität Bonn, 53121 Bonn, Germany. ⁶⁰ Department of Physics, Willamette Uni-
320 versity, Salem, OR 97031, USA. ⁶¹ Institució Catalana de Recerca i Estudis Avançats (ICREA),
321 Barcelona, Spain. ⁶² NASA Postdoctoral Program Fellow, USA. ⁶³ Centre for Space Research,
322 North-West University, Potchefstroom Campus, Private Bag X6001, 2520 Potchefstroom, South
323 Africa. ⁶⁴ Consorzio Interuniversitario per la Fisica Spaziale (CIFS), I-10133 Torino, Italy. ⁶⁵
324 Dipartimento di Fisica, Università di Roma “Tor Vergata”, I-00133 Roma, Italy. ⁶⁶ Department
325 of Physics, Stockholm University, AlbaNova, SE-106 91 Stockholm, Sweden. ⁶⁷ The Oskar
326 Klein Centre for Cosmoparticle Physics, AlbaNova, SE-106 91 Stockholm, Sweden.

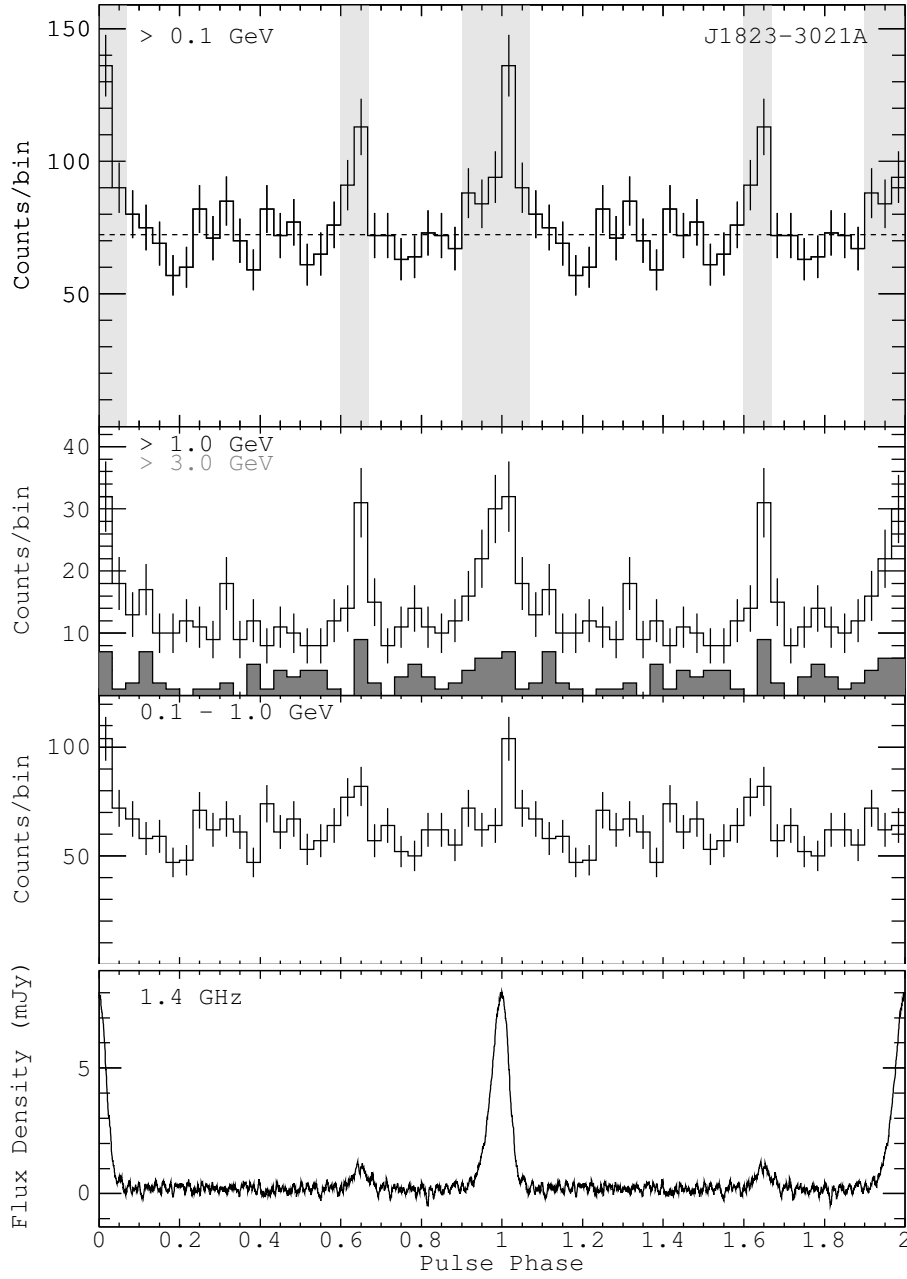


Figure 1: Phase-aligned radio and γ -ray profiles for J1823–3021A. (Bottom) Nançay 1.4 GHz radio profile. (Top and middle) γ -ray profiles obtained with the Fermi-LAT in different energy bands. The dark histogram is for events with $E > 3.0\text{ GeV}$. The γ -ray background for the 0.1 GeV light curve was estimated from a surrounding ring, and it is indicated by the dashed horizontal line in the top panel. The highlighted area there shows the on-pulse region selection.

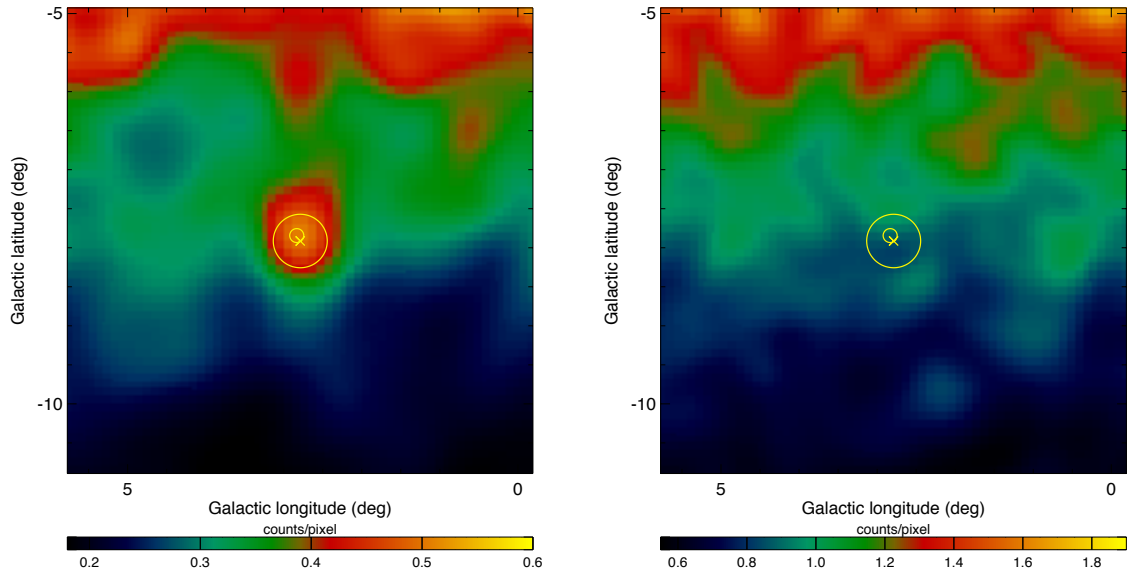


Figure 2: Fermi LAT γ -ray count map above 100 MeV for J1823–3021A during the on-pulse (Left) and off-pulse (Right) regions, as defined in Fig. 1. The 6° by 6° region is centered on the pulsar position (cross). The map was adaptively smoothed by imposing minimum signal-to-noises ratios of 13 and 16 for the on- and off-pulse regions, respectively. The large circle indicates the tidal radius of NGC 6624. The small circle shows the 99% confidence region for the location of the γ -ray source.

327 **Supporting Online Material**

328 **Observations and data analysis**

329 **Radio Timing analysis**

330 With the express purpose of supporting the Fermi mission (33), J1823–3021A is observed
331 approximately 3 times per month with the 76-m Lovell telescope (34), using a 64 MHz band
332 centered at 1404 MHz connected to an analog filterbank. Since mid-2009 observations have also
333 been performed using a digital filterbank backend with 1024×0.5 MHz channels of which ap-
334 proximately 250 MHz is used. Highly precise timing measurements are also conducted with the
335 Nançay radio telescope (35). These have included regular observations of J1823–3021A since
336 mid-2006. Approximately every two months, the pulsar is observed for 1 hour at 1.4 GHz.
337 A 128 MHz bandwidth is coherently dedispersed using powerful GPUs (Graphics Processing
338 Units). A total of 104 pulse times of arrival (TOAs) were obtained from the two telescopes
339 between mid-2006 and mid-2010. The TEMPO2 timing package (36) was used to build the
340 timing solution, which includes the pulsar rotation frequency and its derivatives, the dispersion
341 measure, and the pulsar position. The post-fit residuals are characterized by a weighted rms of
342 $7.3 \mu\text{s}$. The resulting parameters are summarized in Table S1. No trends are noticeable in the
343 post-fit residuals.

344 **Fermi LAT data analysis**

345 We have observed J1823–3021A with the Large Area Telescope aboard Fermi from 2008 Au-
346 gust 4, when the satellite began scanning-mode operations, to the end of the validity range of the
347 pulsar radio ephemeris (2010 October 14). The data analysis presented in this paper has been
348 performed using the LAT Science Tools package 09-21-00 and the P6 V3 Diffuse instrument
349 response functions (IRFs). Events tagged “Pass 6 diffuse” having the highest probability of

350 being γ -ray photons (37) and coming from zenith angles $< 100^\circ$ (to reject atmospheric γ -rays
351 from the Earth’s limb) were used. Additionally, a rotational phase was assigned to each selected
352 LAT event using the radio ephemeris as an input to the Fermi plugin (38) distributed with the
353 TEMPO2 pulsar timing software.

354 Using the `pyLikelihood` likelihood fitting tool with the `NewMinuit` optimizer, we per-
355 formed a binned spectral analysis to determine the energy flux and the spectral shape of the
356 source. Events in the range 0.1–100 GeV were extracted from a $20^\circ \times 20^\circ$ square region of in-
357 terest (ROI) centered on the pulsar position. To reduce the effect of the Earth’s atmospheric
358 emission, the time intervals when the Earth was appreciably within the field of view (specifi-
359 cally, when the center of the field of view was more than 52° from the zenith) were excluded
360 from this analysis. The Galactic diffuse emission was modeled using the *gll_iem_v02* map cube,
361 while the extragalactic emission and residual instrument backgrounds were modeled jointly by
362 the isotropic component *isotropic_iem_v02*. These two models are available from the Fermi
363 Science Support Center¹. In addition, all the sources found in an internal catalog based on 18
364 months of data (similar to (39)) above the background with significances $> 5\sigma$ and within 20°
365 from the pulsar were included in the model. Sources were modeled with a power law spectrum,
366 except for pulsars for which a power law with an exponential cut-off was used (40). Sources
367 more than 5° from the pulsar were assigned fixed spectra taken from the source catalog. Spectral
368 parameters for sources within 5° of the pulsar were left free for the analysis.

369 The pulsar location at the core of NGC 6624 is located just outside the 99% statistical
370 error contour of the γ -ray source 1FGL J1823.4–3009 (39), based on an analysis of the first
371 11 months of the LAT survey data. Therefore, (41) did not establish an association between
372 1FGL J1823.4–3009 and the globular cluster. (42), using a larger dataset, showed that the
373 γ -ray position lies within the (20.55′) tidal radius of the cluster. To check the association,

¹<http://fermi.gsfc.nasa.gov/ssc/data/access/lat/BackgroundModels.html>

374 we first reevaluated the position of the γ -ray source 1FGL J1823.4–3009, using the on-pulse
 375 ($0.60 < \phi < 0.67$ and $0.90 < \phi < 0.07$) segment of the pulsar rotational phase (to improve
 376 the signal-to-noise ratio), to be ($\alpha_{2000} = 275.87^\circ$, $\delta_{2000} = -30.29^\circ$) with a 99% confidence
 377 error radius of 0.09° . This places the pulsar radio position just inside the 99% error contour
 378 of the γ -ray source. We also investigated the off-pulse window and detected a $\sim 4\sigma$ point
 379 source which coincides with the position of the radio source NVSS J182324–300311 ($\alpha_{2000} =$
 380 275.8515° , $\delta_{2000} = -30.053278^\circ$). The signal, only observed during the first year of the Fermi
 381 mission, is located 0.11° away from the position of 1FGL J1823.4–3009 and 0.31° away from
 382 NGC 6624. It is likely that 1FGL J1823.4–3009, located between NVSS J182324–300311 and
 383 NGC 6624, includes contributions from both of these sources. Using the second year of data,
 384 when the nearby faint source is off, we localize the γ -ray source corresponding to the pulsar to
 385 ($\alpha_{2000} = 275.93^\circ$, $\delta_{2000} = -30.34^\circ$) with a 68% error counter radius of 0.07° . This position is
 386 consistent with the radio pulsar position. We then fitted the spectrum of the pulsar at the radio
 387 pulsar position using a power law with an exponential cut-off. Figure S1 shows both the fit
 388 between 0.1 and 30 GeV (solid lines) and the spectral points derived from likelihood fits to each
 389 individual energy band in which it was assumed the pulsar had a power-law spectrum.

390 **Light Curve Modeling**

391 There have been two major contenders for modeling the high-energy (HE) radiation (roughly
 392 100 MeV to 10 GeV range) from pulsars, those which assume that the observed γ -rays are emit-
 393 ted near the stellar surface (43, 44) above the magnetic polar cap and those which assume the
 394 γ -rays originate primarily in the outer magnetosphere near the light cylinder (the distance from
 395 the rotation axis $\vec{\Omega}$ at which the co-rotation equals the speed of light). Both classes of models
 396 assume that the HE γ -rays are curvature radiation from highly-relativistic electrons/positrons in
 397 the radiation-reaction regime. The two most common outer-magnetospheric emission models

398 are the outer gap (OG; (45, 46, 47)) and the slot gap (48) models. For our purposes we took the
 399 two-pole caustic (TPC; (49)) model to be a geometric realization of the slot gap. TPC and OG
 400 models both assume that the emitting electrons are accelerated up to high altitudes in narrow
 401 gaps along the last-open field lines. The OG model only allows acceleration above the null-
 402 charge surface (NCS; where $\vec{\Omega} \cdot \vec{B} = 0$) whereas in the TPC model electrons are accelerated
 403 from the stellar surface. The HE pulse profiles in these outer-magnetospheric models are the re-
 404 sult of the accumulation of photons in narrow phase bands due to a combination of three effects:
 405 aberration (change of photon direction due to the high corotation velocity), time-of-flight de-
 406 lays (photons produced at higher altitudes will reach an observer earlier than those coming from
 407 lower altitudes), as well as the magnetic field line curvature (photons are assumed to be created
 408 tangential to the local magnetic field line in the corotating frame, and their direction is therefore
 409 very sensitive to the magnetic field geometry). This is referred to as caustic emission (50).

410 TPC and OG models are generally used in conjunction with a low-altitude radio cone beam
 411 geometry (e.g., (51, 52)). Due to the difference in altitude of the radio and γ -ray emission, there
 412 will be a phase lag between the radio and γ -ray profiles. Polar-cap (e.g., (44)) γ -ray emission
 413 models do predict much smaller phase lags but, due to the large open field line region of MSPs,
 414 they cannot produce the narrow peaks observed in the γ -ray light curve of PSR J1823–3021A.
 415 The phase-alignment of PSR J1823–3021A’s radio and γ -ray light curves argues for overlap-
 416 ping γ -ray and radio emission regions. To reproduce the phase-aligned light curves we used
 417 altitude-limited versions of the TPC and OG models (aTPC and aLOG, respectively) which
 418 were first introduced to model the light curves of the MSP PSR J0034–0534 (53). These are
 419 very similar to the standard TPC and OG models, except that the minimum and maximum radii
 420 of the radio emission region as well as the maximum radius of the γ -ray emission region are free
 421 parameters (the minimum γ -ray emission radius being set by the standard models). Therefore,
 422 both radio and γ -ray photons originate in a TPC or OG-like structure, with a significant amount

423 of overlap between the two emitting regions leading to phase-aligned profiles. This implies
 424 that the radio emission is also caustic in nature, supported by polarimetric observations which
 425 find 0% linear polarization for PSR J1823–3021A (54). Conversely, these models provide a
 426 framework to constrain the respective radio and γ -ray emission geometries when comparing the
 427 model light curves to the data.

428 We have simulated γ -ray and radio light curves using alTPC and aLOG models with a spin
 429 period $P = 1.5$ ms, steps of 1° in magnetic inclination angle (α) and viewing angle (ζ), 0.05
 430 in accelerating emission layer width (w , normalized to the opening angle of the polar cap),
 431 and 0.10 (in units of $R_{LC} = cP/(2\pi)$) for the emission altitudes. The spin period used in
 432 the simulation is less than that of PSR J1823–3021A (5.44 ms) but this quantity enters the
 433 simulation mainly through the size of the polar cap. Using models with a shorter period will, at
 434 most, overestimate any predicted off-pulse region. We have developed a Markov chain Monte
 435 Carlo (MCMC) maximum likelihood technique to jointly fit the γ -ray and radio profiles and
 436 pick the best-fit parameters (55). We fit the ≥ 500 MeV γ -ray light curve in 60 bins and rebinned
 437 the radio profile to 60 bins. For the γ -ray models the minimum emission altitudes (R_{min}^γ) were
 438 specified as described previously while the maximum emission altitudes were allowed to be free
 439 under the constraint $R_{max}^\gamma \geq 0.7 R_{LC}$. The radio emission altitudes are unconstrained save that
 440 $R_{max}^R > R_{min}^R$. The best-fit parameters for both models are given in Table S2; the likelihood
 441 does not prefer one model over another. The alTPC model has best-fit gap widths of 0.0. This
 442 is unphysical and should be taken to indicate that the true gap widths are between 0.0 and
 443 0.05. Following (52) we can estimate the beaming factor (f_Ω) for both models using Eq. 4
 444 of (51), see Table S2. Presently we are unable to provide reliable uncertainty estimates for our
 445 model predictions and, thus, can not propagate any uncertainty on f_Ω into the uncertainty on
 446 L_γ . However, while PSR J1823–3021A stands out in some respects, the shape of the observed
 447 HE light curve is very typical of known γ -ray MSPs. The best-fit geometries of (55) to these

448 MSPs yield values of f_{Ω} from approximately 0.3 to 1.8, with mean of 0.81 and rms of 0.36. We
449 therefore expect the f_{Ω} value for J1823–3021A to be similar to the geometries which, in these
450 models, produce “typical” γ -ray light curves. The high and low tails of this distribution suggest
451 that the γ -ray efficiency could reasonably be anywhere from 3 to 20% but neither extreme
452 affects the conclusion of the main text that most of the observed \dot{P} is intrinsic to the pulsar.

| Timing parameters | |
|--|---|
| Right Ascension, α (J2000) | 18 ^h 23 ^m 40 ^s .48466(4) |
| Declination, δ (J2000) | −30° 21′ 39″.988(4) |
| Solar System Ephemeris | DE 405 |
| Reference time scale | TDB |
| Reference time (MJD) | 54939 |
| Spin Frequency, ν (Hz) | 183.823389814514(7) |
| First derivative of ν , $\dot{\nu}$ (10^{-15} Hz s ^{−1}) .. | −114.1351(4) |
| Second derivative of ν , $\ddot{\nu}$ (10^{-25} Hz s ^{−2}) | 5.8(1) |
| Dispersion Measure, DM (cm ^{−3} pc) | 86.864(9) |
| Validity Range (MJD) | 53773.35 – 55483.67 |
| RMS Timing Residuals (μ s) | 7.3 |

Table S1. Timing parameters for J1823–3021A. The center of the globular cluster is located at $\alpha = 18^{\text{h}}23^{\text{m}}40^{\text{s}}:51 \pm 0^{\text{s}}:008$, $\delta = -30^{\circ}21'39''.7 \pm 0''.1$.

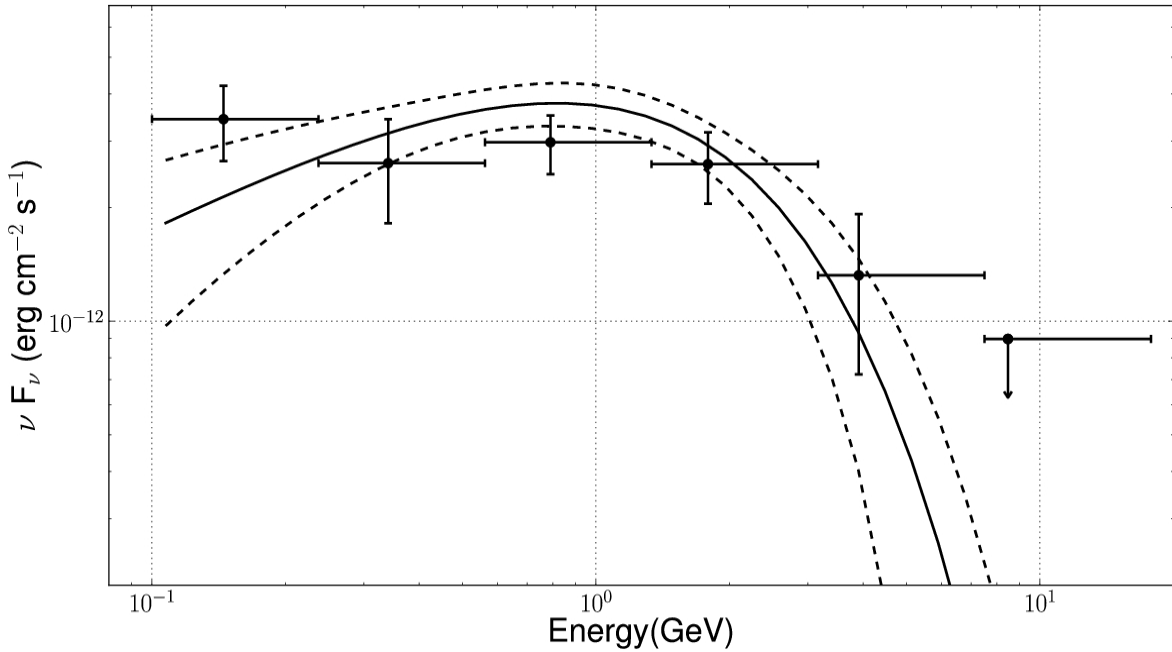


Fig. S1. γ -ray spectral energy distribution of J1823–3021A obtained with the Fermi Large Area Telescope. The solid black line shows the maximum likelihood fit to a power law with exponential cut-off. The dashed lines are $\pm 1\sigma$ uncertainties on the fit parameters. Plotted points are from likelihood fits to individual energy bands with $> 3\sigma$ detection above background for two degrees of freedom, otherwise a 95% confidence level upper limit arrow is shown. The errors are statistical only.

| Best-fit Light Curve Parameters | | | | | | | | | | |
|--|----------------------|--------------|-------------------------|------------------------|--------|--------------|----------------|--------------------|------------------------------|----------------------|
| Model | $-\log(\text{Like})$ | f_{Ω} | α ($^{\circ}$) | ζ ($^{\circ}$) | Φ | w_{γ} | w_{R} | R_{max}^{γ} | R_{min}^{R} | R_{max}^{R} |
| aTPC | 173.8 | 0.9 | 51 | 68 | 0.017 | 0.00 | 0.00 | 1.0 | 0.2 | 0.9 |
| aIOG | 173.6 | 0.9 | 69 | 68 | 0.017 | 0.05 | 0.10 | 1.2 | $max\{R_{\text{NCS}}, 0.2\}$ | 0.8 |

Table S2. Results of MCMC maximum likelihood fits to the γ -ray and radio light curves of PSR J1823–3021A using the aTPC and aIOG models.

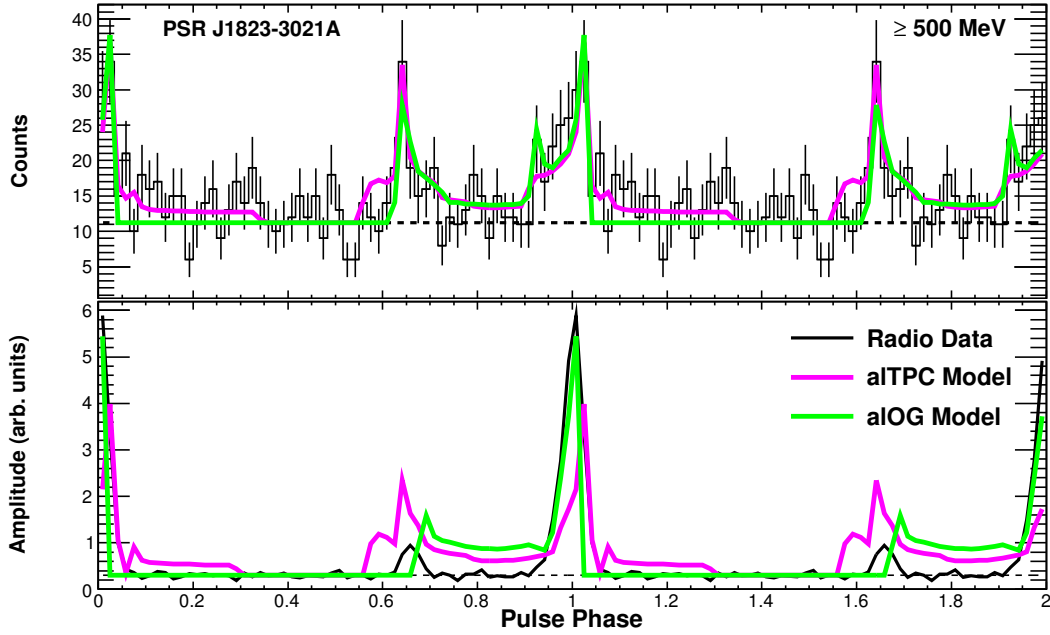


Fig. S2. Observed and best-fit γ -ray (top) and radio (bottom) light curves for PSR J1823–3021A using the aITPC (pink) and aLOG (green) models described in the text. The dashed, horizontal lines in both panels correspond to the estimated background levels. The γ -ray background was estimated using an annular ring centered on the radio position with inner and outer radii of 1° and 2° , respectively. The radio background was estimated by fitting the region between 0.1 and 0.6 in phase to a constant value. The parameters of the best-fit light curves are given in Table S2.